Int J CARS (2010) 5:385–391
DOI 10.1007/s11548-010-0415-x

ORIGINAL ARTICLE

C-arm rotation encoding with accelerometers

Victor Grzeda · Gabor Fichtinger

Received: 11 January 2010 / Accepted: 24 March 2010 / Published online: 10 April 2010

Abstract
Purpose Fluoroscopic C-arms are being incorporated in computer-assisted interventions in increasing number. For these applications to work, the relative poses of imaging must be known. To find the pose, tracking methods such as optical cameras, electromagnetic trackers, and radiographic fiducials have been used—all hampered by significant shortcomings.
Methods We propose to recover the rotational pose of the C-arm using the angle-sensing ability of accelerometers, by exploiting the capability of the accelerometer to measure tilt angles. By affixing the accelerometer to a C-arm, the accelerometer tracks the C-arm pose during rotations of the C-arm. To demonstrate this concept, a C-arm analogue was constructed with a webcam device affixed to the C-arm model to mimic X-ray imaging. Then, measuring the offset between the accelerometer angle readings to the webcam pose angle, an angle correction equation (ACE) was created to properly tracking the C-arm rotational pose.
Experiments and results Several tests were performed on the webcam C-arm model using the ACEs to tracking the primary and secondary angle rotations of the model. We evaluated the capability of linear and polynomial ACEs to tracking the webcam C-arm pose angle for different rotational scenarios. The test results showed that the accelerometer could track the pose of the webcam C-arm model with an accuracy of less than 1.0 degree.
Conclusion The accelerometer was successful in sensing the C-arm's rotation with clinically adequate accuracy in the C-arm webcam model.

Keywords C-arm · Encoding · Accelerometer

V. Grzeda (✉) · G. Fichtinger
Laboratory for Percutaneous Surgery, School of Computing, Queen's University, Kingston, ON, Canada
e-mail: grzeda@cs.queensu.ca; vicgrz@shaw.ca

G. Fichtinger
e-mail: gabor@cs.queensu.ca

Introduction

Fluoroscopic C-arms have been an important tool in computer-assisted interventions. The basic use of a fluoroscopic C-arm in computer-assisted applications is to reconstruct anatomical structures and objects into 3D from their 2D X-ray images. Reconstruction requires the relative pose of the 2D projection images to be known, a problem commonly known as C-arm pose tracking.

Accurate, practical, and affordable C-arm pose tracking is a major technical challenge. There are motorized C-arm devices that provide rotational pose information, but they are rather expensive and susceptible to pose errors due to wheel motion, sagging, and deformation of the device. Conventional manual C-arms are supplanted with some tracking method to recover the C-arm pose. Tracking may take two forms, external or X-ray image based. In external tracking, an object called a dynamic reference body (DRB) is attached to the C-arm, while the pose of the DRB is sensed by optical cameras or electromagnetically [7]. External tracking produces full six degrees of freedom (DOF) pose of the C-arm and is resistant to wheel motion, sagging, and deformation of the C-arm. Optical tracking is usually more accurate but requires line of sight. Electromagnetic tracking does not demand line of sight but is susceptible to field distortions typically caused by the presence of metallic objects or even the earth's magnetic field. A further shortcoming is that prior to using the system the DRB needs to be pre-calibrated to

the C-arm image. In all, external tracking tends to add significant cost and complexity to the system. In image-based tracking, a radio-opaque object of known geometry (commonly referred as fiducial) is placed in the field of imaging [5,11]. If the fiducial has sufficient specificity, then the full 6 DOF pose of the C-arm image can be computed relative to the fiducial. While image-based tracking is inexpensive and potentially accurate, the fiducial occupies valuable real estate in the fluoroscopic image.

An alternative tracking method is the use of accelerometers to recover the pose. The initial theory postulated the use of accelerometers as a positional tracker, by performing a double integration of the acceleration information to retrieve positional information. Several previously published papers have used accelerometers in position tracking mainly for robotic applications [1,8,9]. However, applying similar methodologies to recover the C-arm pose proved problematic. Setting aside the inherent issues with accelerometers, such as noise, bias, and drift [10,12], the mechanical properties of the C-arm did not allow for the accelerometer positional tracking methods to perform to an acceptable level of accuracy. The main issue stems from the C-arm rotations, shown in Fig. 1. The accelerometer senses motion and gravity forces. This means that when the C-arm rotates along its primary or secondary axis, the accelerometer will output readings containing both forces. This makes it extremely difficult to discern the true motion required for pose tracking. If the accelerometer is coupled with a gyroscope, it will give orientation, which helps to isolate the effects of static gravity. Knowing the static gravity, it can be subtracted from the accelerometer readings, thereby giving true motion acceleration at each time interval. This is a very complex and potentially costly strategy.

Since accelerometers can accurately measure the force of gravity and the accelerometer has known geometric properties, we can reconfigure the device into a tilt (angle) sensor. In this paper, we propose and evaluate a new technique to recover the fluoroscopic C-arm rotation pose using the angle-sensing capabilities of an accelerometer.

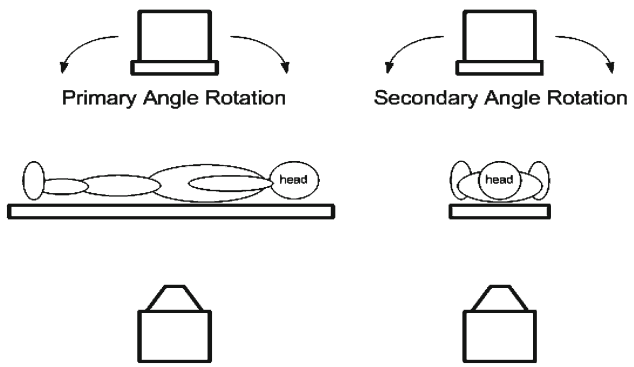

Fig. 1 C-arm rotational axes relative to the placement of patient

The driving clinical application for our work is intra-operative implant reconstruction in prostate cancer brachytherapy [3]. In this application, the C-arm is operated in a step-and-shoot mode with a severely limited rotational angle. This limitation is approximately a 40-degree cone about the canonical vertical pose of the C-arm, where both rotational axes of the C-arm move between ±20 degrees. Factors that create this constrain are potential collision with patient, operating room table, and other standard instrumentation used in the procedure. For successful reconstruction of the brachytherapy implants, the C-arm pose needs to be recovered with an accuracy of about 1.0 degree [3,7].

Methods

Accelerometer

The key to the proposed technique is an accelerometer. These devices are small, low cost, and have low power requirements, which allow them to be self-contained sensing systems. While they can be custom made for a desired application, many general purpose packages are widely available ranging from 1, 2, and 3 DOF sensors. The most common use of accelerometers are in inertial measurement units for determining orientation (roll, pitch, and yaw), which we also use to find the C-arm pose. The principle behind our approach begins with each axis measuring the influence of gravity. In a stable state with no motion force, each axis will measure a component of the overall gravity force of 1g, shown in Eq. 1. Knowing this property, calculating the desired angles is a matter of taking the appropriate ratios of the accelerometer values from each axis [2]. Equation 2 gives an example, where α is the angle along x-axis and β is the angle along the y-axis. Also the z-axis is the common gravity axis that can be change depending on the chosen orientation of the accelerometer mounted on the C-arm.

$$\sqrt{A_x^2 + A_y^2 + A_z^2} = 1g \tag{1}$$

$$\alpha = \tan^{-1}\left(\frac{A_x}{\sqrt{A_y^2 + A_z^2}}\right) \quad \beta = \tan^{-1}\left(\frac{A_y}{\sqrt{A_x^2 + A_z^2}}\right) \tag{2}$$

In our experimental prototype, we used a Sparkfun™ Electronics WiTilt v3 packaged device. It is intended for general purpose applications containing a Freescale MMA7260Q triple-axis accelerometer with a class 1 Bluetooth® communication link. The small package allows for placing the accelerometer on the detector or source without interfering with normal use of the C-arm, and the wireless communication does not intrude upon the operating room. For convenience, we align the accelerometer axes approximately with the rotational axes of the C-arm.

C-arm analogue

To evaluate the concept on an actual C-arm would involve harmful ionizing radiation. To reduce the laboratory turn-around time and eliminate radiation exposure, we constructed a radiation-free downscaled model of the C-arm. The model shown in Fig. 2 (*left*) mimics the mechanical rotations of a full size clinical C-arm. To mimic X-ray imaging, we attached a Microsoft LifeCam VX-3000 webcam to the top end of the C-arm analogue. Just as X-ray imaging, optical imaging creates 2D images even though the principle of their imaging modalities is different. Creating a 2D image involves using a source and apparatus to capture the image, shown in Fig. 2 (*right*). In X-ray imaging, photons are expelled from the point source. The photons travel in a straight line through the target and hit the detector to create a 2D shadow of the target. Optical imaging uses the same geometrical principle, but the photons of visible light reflect off the target traveling in a straight line towards the camera. Calculating the angle of image is comparable in both modalities since the structure of the C-arm is maintained.

Calibration

Our proposed technique requires the calibration of the accelerometer to the rotation axes of the C-arm. The calibration requires an independent pose tracking ground truth, provided by either external tracker or tracking fiducial. We intend to use the fluoroscope tracking fiducial (FTRAC) developed by Jain et al. [6]. Then, the accelerometer pose estimate can be compared directly to this ground truth. Figure 3 shows the flowchart of C-arm pose tracking using the accelerometer angle-sensing ability.

The apparent straightforwardness of the idea should not belie the investment of effort needed to make it a workable clinical tool. One of the most important aspects is the initial

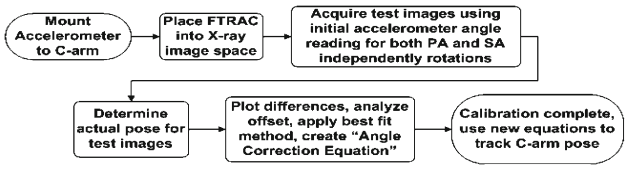

Fig. 3 The steps for C-arm pose tracking with accelerometer. *PA* primary angle, *SA* secondary angle

mounting of the accelerometer to the C-arm. As mentioned earlier, the small device packaging makes it ideal and convenient to place on the C-arm detector or source. By properly securing and calibrating the device, subsequent uses will continue to be valid with the computed calibration offset. Next, several test images need to be taken using the initial reading of the accelerometer. This is important since these readings will determine the offset between the C-arm pose and accelerometer. When choosing these test angles, it is imperative to ensure that the angles have enough separation and a sufficiently wide range to account for possible variations of the primary and secondary angles (PA and SA) when the C-arm is in motion. The final step is to calculate the actual C-arm pose of these test images using the ground-truth tracker and analyse the differences between the ground-truth and the initial accelerometer angle readings. Then, applying a best-fit method to the primary and secondary angle (PA and SA, respectively) errors, we obtain the quantifiable offset termed angle correction equation (ACE), which completes the calibration of the accelerometer to the C-arm.

The intended purpose of the technique is for use on a fully functional fluoroscopic C-arm as described. However, our evaluation of the technique was performed on a C-arm analogue with the necessary substitutions. The experimental setup is shown in Fig. 4, with a checkerboard (acts as FTRAC) placed on top of a case stand that is near the centre point of the C-arm. The webcam (mimics X-ray source/detector) is

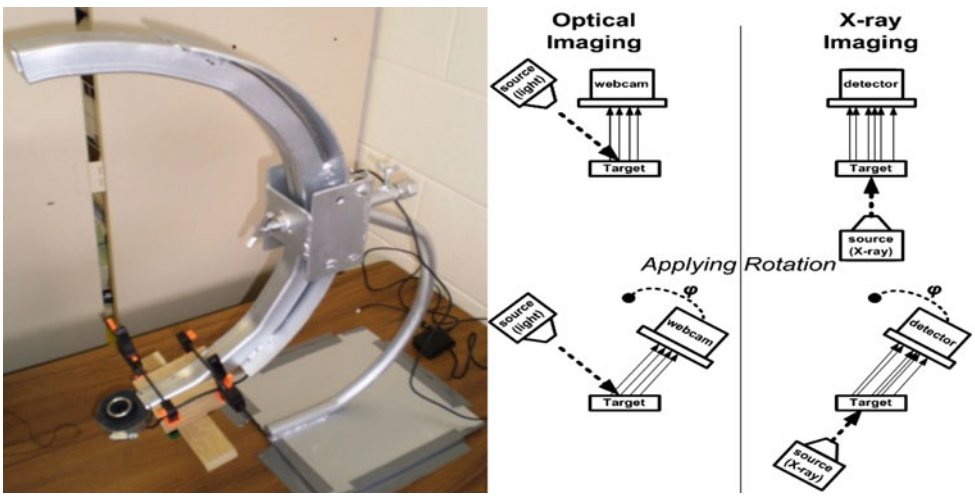

Fig. 2 *Left*: C-arm analogue instrumented with webcam. Note that the C-arm is currently upside-down to better view the construction of the C-arm. *Right*: How 2D images are created in X-ray and optical imaging modalities and their similarities during rotations

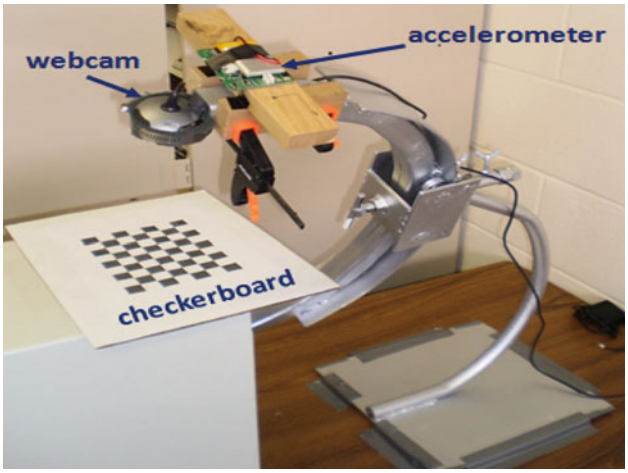

Fig. 4 Experimental setup for the C-arm analogue with checkerboard plate for calibration and ground-truth for pose tracking

mounted on the top end of the C-arm analogue with the accelerometer placed above. A MATLAB program was created to read the acceleration measurements from the accelerometer. Then, the angle is computed by creating a set of 50 measurements, which is filtered using a robust local regression smoother to reduce the influence noise to create consistent acceleration signal. After filtering, the mean value of the set is taken for each axis of the accelerometer. The angle is computed using similar equations to Eq. 1 and Eq. 2, which is then displayed on-screen. For rotational pose calibration, 20 primary angles (PA) and 20 secondary angles (SA) were taken at random angles to compute the intrinsic and extrinsic camera parameters. Camera calibration was achieved by a MATLAB toolbox.

Following the steps outlined in the technique, we needed to determine the offset between the initial accelerometer angle reading and the webcam C-arm pose. A sample angle set for the test images were taken at $[0° \pm 4° \pm 8° \pm 12° \pm 16° \pm 20°]$ for PA and SA independently giving an evenly spaced wide range of angles for experimentation. This was chosen based on the constraints of clinical application motivating this work. Each image was taken in a step-and-shoot mode as well.

To calculate the ground-truth angles, the intrinsic parameter, computed in the camera calibration setup, was used to compute the extrinsic parameter for each test image. Within the extrinsic parameter is a rotational matrix that corresponds to the transform between the 2D-image to its 3D-orientation. When this matrix is broken down into individual angular components, they can be interpreted as the actual angle for the PA and SA [2], respectively. The initial offset between the accelerometer and webcam pose is shown in Table 1, with the differences obtained by subtracting the initial accelerometer angle reading from the actual webcam C-arm pose angle.

To better interpret the error shown in Table 1, we created the plots shown in Fig. 5 (*left*). The data points were fitted with least square optimization to straight lines shown in Fig. 5 (*right*). It was posited that the fitting resulted in a quantifiable offset in form of an angle correction equation (ACE). The ACEs for the PA and SA are expressed in Eqs. 3 and 4, respectively.

Let x represent the initial *PA* accelerometer reading, then the new

$$PA^* = 1.027 \cdot x + 1.734 \tag{3}$$

Let z represent the initial *SA* accelerometer reading, then the new

$$SA^* = 1.009 \cdot z + 1.381 \tag{4}$$

The linear best-fit method to create the ACEs is not the only option. As an alternative a more complex polynomial fit was applied to the data, shown in Fig. 6. This creates

Table 1 The initial offset calibration showing the differences between initial accelerometer angles and actual webcam pose angles

Initial accelerometer readings	Primary angle (PA)		Secondary angle (SA)	
	Actual webcam pose angles	Differences	Actual webcam pose angles	Differences
20	22.33	2.33	18.73	−1.27
16	18.22	2.22	14.78	−1.22
12	14.03	2.03	10.89	−1.11
8	9.85	1.85	6.69	−1.31
4	5.88	1.88	2.59	−1.41
0	1.73	1.73	−1.39	−1.39
–4	−2.36	1.64	−5.61	−1.61
–8	−6.63	1.37	−9.35	−1.35
–12	−10.49	1.51	−13.46	−1.46
–16	−14.56	1.44	−17.33	−1.33
–20	−18.91	1.09	−21.73	−1.73

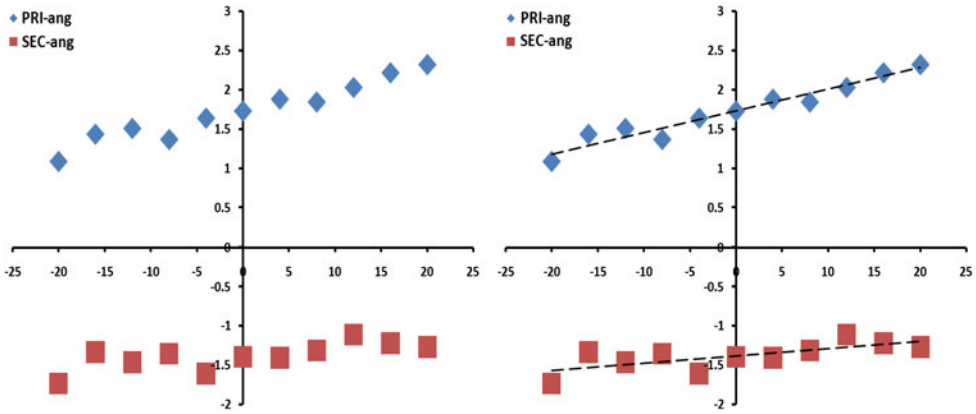

Fig. 5 *Left*: Graphical visualization of the differences between initial accelerometer angles and webcam angles. *Right*: Linear best fit over the data points creating ACEs for PA (Eq. 3—$R^2 = 0.94$) and SA (Eq. 4—$R^2 = 0.51$)

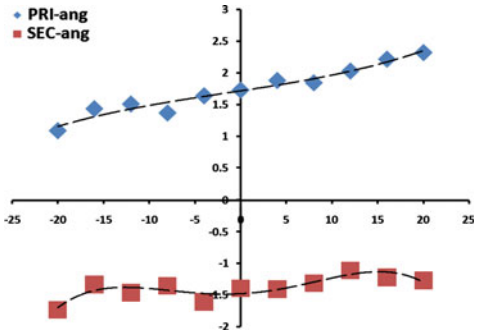

Fig. 6 Polynomial fitting applied to the initial offset differences of Table 1 creating ACEs for PA (Eq. 5 with $R^2 = 0.95$) and SA (Eq. 6 with $R^2 = 0.80$)

new polynomial fit lines with the associated ACEs, Eqs. 5 and 6. The principle behind the equations is a conversion process from the initial accelerometer angle reading to a corrected accelerometer angle output, which will correspond to the webcam C-arm analogue pose angle.

Let x represent initial *PA* accelerometer reading, then the new

$$PA^* = 2E^{-05} \cdot x^3 + 9E^{-05} \cdot x^2 + 1.022 \cdot x + 1.734 \quad (5)$$

Let z represent initial *SA* accelerometer reading, then the new

$$SA^* = -6E^{-06} \cdot z^4 + 6E^{-06} \cdot z^3 + 0.002 \cdot z^2 + 1.008 \cdot z + 1.478 \quad (6)$$

Tests and results

In order to characterize how accurately the ACEs can track the webcam C-arm pose, we performed a series of tests. For the first test, we judged whether ACEs were a viable method for tracking by changing the angular settings for PA and SA test images to [0° ± 2° ± 6° ± 10° ± 14° ± 18°]. The new angle set avoids using the same angles that we used for creating the ACEs, in order witness if the ACEs can interpolate the in-between angles. The linear ACE accelerometer readings and actual webcam pose are shown in Table 2, with the error differences obtained by subtracting the ACE accelerometer angle from the actual webcam C-arm pose angle.

As a second test, we examined the diagonal angles where both the PA and SA were rotated together to determine if the ACEs were able to maintain correct tracking of the pose. For this test, the angle set reverted back to original [±4° ± 8° ± 12° ± 16° ± 20°], but as pairs of both PA and SA. Table 3 shows the mean and standard deviation of the error differences for the PA and SA, in each respective quadrant. A test angle used was [+4,−4], that is, positive four degrees for PA and negative four degrees in SA.

For the final test we examined the alternative ACEs created using the polynomial fit method. The angle set for test images remained the same as in the previous diagonal test; angles of [0°±4°±8°±12°±16°±20°] for both PA and SA were taken independently. The polynomial ACE accelerometer readings and actual webcam pose are shown in Table 4, with the error differences obtained by subtracting the ACE accelerometer readings from the actual webcam C-arm pose angles.

Discussion and conclusion

We were successful in finding a linear relationship between the webcam C-arm angles and accelerometer angles. According to Table 1 and Fig. 5, it was possible to create an offset equation that properly relates the accelerometer angles to the webcam angles. The results from Table 2 show that using the ACEs, the accelerometer can properly track the webcam pose angle with less than 1° of error. Also of note is Table 3, the accelerometer can simultaneously track the PA and SA with a high degree of reliability, but we lose accuracy for SA during PA negative rotations. This can be attributed to the imprecision of our metal C-arm analogue, because it was rather crudely engineered with the sole objective of mimicking mechanical functionality of the C-arm. When looking at the distribution of the pose of calibration images, the C-arm

Table 2 The ACE accelerometer readings compared to the actual webcam pose angles of the test images

ACE accelerometer readings	Primary angle (PA)		Secondary angle (SA)	
	Actual webcam pose angles	Differences	Actual webcam pose angles	Differences
18	18.68	0.68	18.27	0.27
14	14.67	0.67	14.08	0.08
10	10.66	0.66	10.12	0.12
6	6.66	0.66	6.19	0.19
2	2.83	0.83	2.23	0.23
0	0.89	0.89	0.75	0.75
–2	−1.06	0.94	−1.85	0.15
–6	−5.25	0.75	−5.87	0.13
–10	−9.36	0.64	−9.59	0.41
–14	−13.41	0.59	−13.79	0.21
–18	−17.38	0.62	−17.87	0.13
	$\boldsymbol{\mu} = 0.70$	$\boldsymbol{\sigma} = 0.11$	$\boldsymbol{\mu} = 0.19$	$\boldsymbol{\sigma} = 0.10$

Table 3 The means (μ)and standard deviations (σ) for the diagonal angle test, which is separated into four quadrants

	Angle difference error			
	+PA		−PA	
	PA	SA	PA	SA
−SA	$\mu = 0.01$ $\sigma = 0.13$	$\mu = 0.26$ $\sigma = 0.31$	$\mu = 0.02$ $\sigma = 0.37$	$\mu = 1.90$ $\sigma = 0.34$
+SA	$\mu = 0.41$ $\sigma = 0.17$	$\mu = 0.04$ $\sigma = 0.17$	$\mu = 0.46$ $\sigma = 0.06$	$\mu = 1.25$ $\sigma = 0.26$

Table 4 Polynomial ACE pose tracking

ACE accelerometer readings	Primary angle (PA)		Secondary angle (SA)	
	Actual webcam pose angles	Differences	Actual webcam pose angles	Differences
20	20.53	0.53	22.31	2.31
16	16.39	0.39	17.56	1.56
12	12.34	0.34	13.37	1.37
8	8.12	0.12	9.27	1.27
4	4.06	0.06	5.05	1.05
0	0.51	0.51	0.83	0.83
–4	−4.13	−0.13	−3.27	0.73
–8	−8.11	−0.11	−7.51	0.49
–12	−12.45	−0.45	−12.05	−0.05
–16	−16.58	−0.58	−16.32	−0.32
–20	−20.47	−0.47	−20.09	−0.09
	$\boldsymbol{\mu} = 0.02$	$\boldsymbol{\sigma} = 0.41$	$\boldsymbol{\mu} = 0.83$	$\boldsymbol{\sigma} = 0.79$

rotations suggest a wobbling trajectory, as shown in Fig. 7. The circled area highlights the most probable causes for the decreased accuracy, since the PA rotational path does not remain straight, slanting into the positive SA direction. This in turn affects the proper tracking of the SA by creating an unaccounted offset.

Using an alternative fit method to create the ACEs produced mixed results. Examining Table 4, the third-order

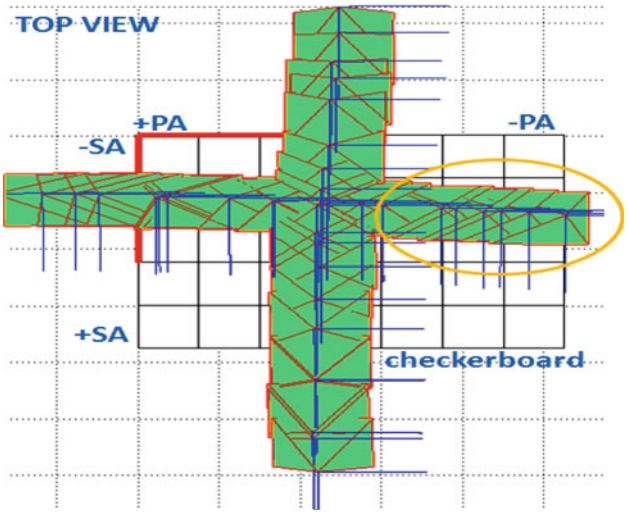

Fig. 7 The distribution of the pose of calibration images for the webcam C-arm metal analogue. The circled highlighted area shows a slanting path during negative PA rotation, which creates an unaccounted for offset when rotating diagonally

polynomial for PA correction helped to improve the accuracy of pose tracking with slightly less precision. However, the fourth-order polynomial for SA correction was unsuccessful in tracking the pose. It shows that in one case a better relationship was found, while in the other the original was better. This introduces a refinement in the ACE creation step of the technique where a testing loop would be added to examine a few fitting methods choosing the best one to use permanently on a C-arm. Still, a simple linear fit method works sufficiently well for our application.

These tests were successful and allow us to progress to an actual C-arm while still using a webcam affixed to either the source or detector, as a substitute for actual X-ray. This scenario will allow us to safely examine the characteristics of a full size C-arm, including deflection, bending, and wheel motion of the C-arm, without exposure to harmful radiation. We expect deflections to arise from the heavy detector and source where the further from vertical the greater the force of gravity creating a bend in the C structure. Another expected shortcoming stems from a most positive feature of the C-arm: its mobility. The C-arm uses wheels and wheel locks to hold the C-arm in place, but as wheel locks are never perfect, they allow for a slight amount of motion when rotating the C-arm. It remains to be seen if the effects from these "rocking" like motions mount to significant pose error.

In conclusion, this paper introduced an alternative tracking method that uses the tilt-sensing capabilities of accelerometers. By placing the accelerometer directly on the C-arm, the goal was to relate the C-arm pose to the accelerometer angle. Our method requires a single calibration step that yields an offset for correction between accelerometer angles and C-arm rotational pose angles. We demonstrated the concept on a radiation-free downscaled C-arm analogue instrumented with a webcam to mimic X-ray imaging. Work continues with an actual C-arm device, with the ultimate objective of a clinically feasible implementation.

References

1. Barshan B, Durrant-Whyte HF (1995) Inertial navigation system for mobile robots. IEEE Trans Robotics Automation 11(2):328–345
2. Batista J, Araujo H, Almeida AT (1996) Pose view stability analysis for camera look angles computation. In: Proceeding of the 13th international conference on pattern recognition (ICPR), pp 171–175
3. Jain A, Deguet A, Iordachita I, Chintalapani G, Blevins J, Le Y, Armour E, Burdette C, Song D, Fichtinger G (2007) Intra-operative 3D guidance in prostate brachytherapy using a non-isocentric C-arm. Med Image Comput Comput Assist Interv 10(Pt 2):9–17
4. Jain A, Fichtinger G (2006) C-arm tracking and reconstruction without an external tracker. Med Image Comput Comput Assist Interv 9(Pt 1):494–502
5. Jain A, Mustafa T, Zhou Y, Burdette C, Chirikjian GS, Fichtinger G (2006) FTRAC—A robust fluoroscope tracking fiducial. Med Phys 32(10):3185–3198
6. Lee J, Liu X, Jain AK, Song DY, Burdette EC, Prince JL, Fichtinger G (2009) Prostate brachytherapy seed reconstruction with Gaussian blurring and optimal coverage cost. IEEE Trans Med Imaging 28(12):1955–1968
7. Peters T, Cleary K (eds) (2008) In: Image-guided interventions: technology and applications, Springer
8. Nikbakht S, Mazlom M, Khayatian A (2005) Evaluation of solid-state accelerometer for positioning of vehicle. In: IEEE internatonal conference on industrial technology (ICIT), pp 729–733
9. Tan CW, Park S (2005) Design of accelerometer-based inertial navigation system. IEEE Trans Instrum Measurement 54(6):2520–2530
10. Thong YK, Woolfson MS, Crowe JA, Hayes-Gill BR, Jones DA (2004) Numerical double integration of acceleration measurement in noise. Measurement 36:73–92
11. Yao J, Taylor RH, Goldberg RP, Kumar R, Bzostek A, Van Vorhis R, Kazanzides P, Gueziec A (2000) A C-arm fluoroscopy-guided progressive cut refinement strategy using a surgical robot. Comput Aided Surg 5(6):373–390
12. Zhang NF (2006) Calculation of the uncertainty of the mean of autocorrelated measurements. Metrologia 43:S276–S281